IEEE Photonics Journal
An IEEE Photonics Society Publication

Compact and Broadband 1 × 4 Optical Switch Based on W2 Photonic Crystal Waveguides

Volume 8, Number 5, October 2016

Qiang Zhao
Kaiyu Cui
Xue Feng
Fang Liu
Wei Zhang
Yidong Huang

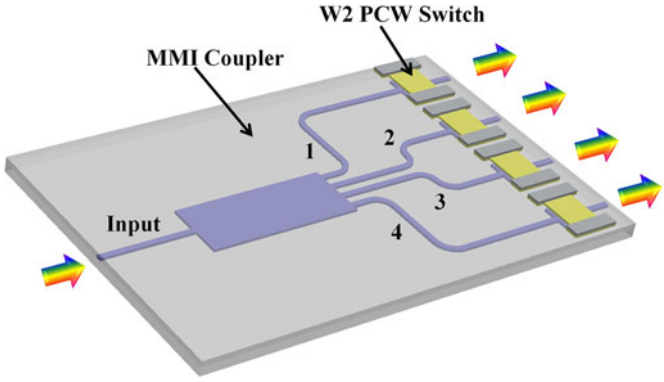

DOI: 10.1109/JPHOT.2016.2611699
1943-0655 © 2016 IEEE

Compact and Broadband 1 × 4 Optical Switch Based on W2 Photonic Crystal Waveguides

Qiang Zhao, Kaiyu Cui, Xue Feng, Fang Liu, Wei Zhang, and Yidong Huang

Department of Electronic Engineering, National Laboratory for Information Science and Technology, Tsinghua University, Beijing 100084, China

DOI:10.1109/JPHOT.2016.2611699

Manuscript received August 4, 2016; revised September 12, 2016; accepted September 17, 2016. Date of publication September 21, 2016; date of current version October 10, 2016. This work was supported in part by the National Basic Research Program of China under Grant 2013CBA01704 and Grant 2013CB328704, in part by the National Natural Science Foundation of China Grant 61307068, and in part by the Opened Fund of the State Key Laboratory on Integrated Optoelectronics under Grant IOSKL2015KF01. Corresponding author: K. Cui (kaiyucui@tsinghua.edu.cn).

Abstract: We demonstrate a compact and broadband 1 × 4 optical switch based on W2 photonic crystal waveguides (PCWs). The footprint of the W2 PCW is only 17.6 μm × 8 μm. An operation bandwidth of 15 nm ± 1 nm is implemented with an extinction ratio over 15 dB in each channel. By introducing the thermal insulation trench, the tuning efficiency is enhanced at least 77% in experiment. The experimental results indicate the potential of the proposed broadband thermo-optic switch in silicon on-chip interconnects.

Index Terms: Multichannel, optical switch, photonic crystals.

1. Introduction

With improvement of the multi-core processor parallel computing technology, the conventional on-chip electrical interconnect becomes bandwidth-limiting and power consuming [1]. On the other hand, the on-chip silicon based optical interconnects have been rapidly developed and provided as a viable alternative for high bandwidth, low power consumption, and compatibility with complementary metal-oxide-semiconductor (CMOS) technology [2]. To provide on-chip reconfigurable communication paths for cores and memory systems, optical routing schemes with high bandwidth capacity have been considered, and the use of aggressive wavelength-division multiplexing (WDM) technology is deemed inevitable [3]–[4].

A key device for on-chip non-wavelength-selective optical routing is the multi-channel optical switch, which is capable of routing data streams in WDM channels [5]–[6]. The switching bandwidth limits the number and spacing of the WDM channels, and thus, broad bandwidth is highly desired for large capacity optical network. Also, the switch should have low crosstalk, low power consumption, relatively small footprint and easily be expanded to large scale. Previously, microring based resonant switches [7] and Mach-Zender interferometer (MZI) based non-resonant switches [4], [8], [9] have been proposed as node devices for on-chip optical routing functions. However, microring based switches are difficult to obtain broad bandwidth due to resonant cavities, while MZI based switches usually have large footprint for long phase shift arms. As a promising candidate for compact photonic

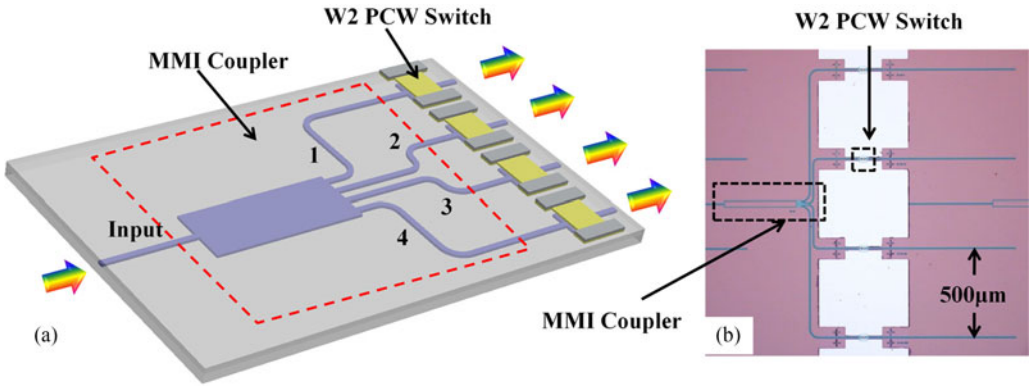

Fig. 1. (a) Schematic structure and (b) optical microscope image of the 1 × 4 broadband optical switch.

devices, photonic crystal waveguide (PCW) based optical switches have been studied extensively over the past few years [10]–[14]. In our previous work, we demonstrated a single channel photonic crystal waveguide (PCW) based broadband optical switch with 24 nm operation bandwidth, which is the most compact broadband PCW switch reported up to now [15].

In this paper, we demonstrate a compact and broadband 1 × 4 PCW based optical switch, which consists of a symmetric 1 × 4 multimode interference (MMI) coupler and four broadband W2 PCW switches. The footprint of a single W2 PCW is only 17.6 μm × 8 μm. With consideration of reducing inter-channel thermal crosstalk for dense multi-channel applications, we introduce silicon dioxide (SiO_2) based thermal insulation trenches with width of 12 μm. As a result, the thermal crosstalk is reduced by 50% in simulations and the tuning efficiency is enhanced at least by 77% in experiment. The measurement of the 1 × 4 PCW based optical switch demonstrates that an operation bandwidth of 15 nm ± 1 nm has been implemented with an extinction ratio over 15 dB for the operating wavelengths in each channel, indicating the potential application in silicon on-chip interconnects.

2. Design and Discussion

Fig. 1(a) shows the schematic structure of the 1 × 4 optical switch. The optical signal is symmetrically split by a 1 × 4 MMI coupler and each output channel is controlled by a thermo-optic PCW switch. Here, MMI based power splitter is chosen for the merit of compact-size, flexible design, low power imbalance, large bandwidth, and high tolerance to fabrication process error [16]. Fig. 1(b) presents the optical microscope image of the switch sample, which is fabricated on a silicon-on-insulator (SOI) platform with a 3-μm-thick buried oxide layer and a 230-nm-thick top silicon layer. The pattern is defined by electron beam lithography (EBL) and inductively coupled plasma (ICP) etching. After dry etching, a 600-nm-thick SiO_2 cladding is deposited on the Si layer by plasma-enhanced chemical vapor deposition (PECVD) for symmetric refractive index contrast distribution in vertical direction. The titanium (Ti)/aluminum (Al) microheater is deposited on each PCW by ultra-violet (UV) lithography and metal evaporation [17]–[18].

Symmetrical 1 × N MMI couplers are commonly used in photonic circuits as beam splitters. Although the maximum power efficiency is only 1/N in each channel, MMI couplers are still the primary broadband beam splitting device for their simple structure, large optical bandwidth, and low excess loss [19]. The basic concept of MMI coupler is the eigenmode interference in multi-mode waveguide, which constructs one or multiple self-images at periodic intervals. Thus the input optical power can be symmetrically split into arbitrary number of outputs with certain waveguide length. Fig. 2(a) shows the optical microscope image of the fabricated 1 × 4 MMI coupler. The detailed scanning electron microscope (SEM) image of the output port is displayed in Fig. 2(b).

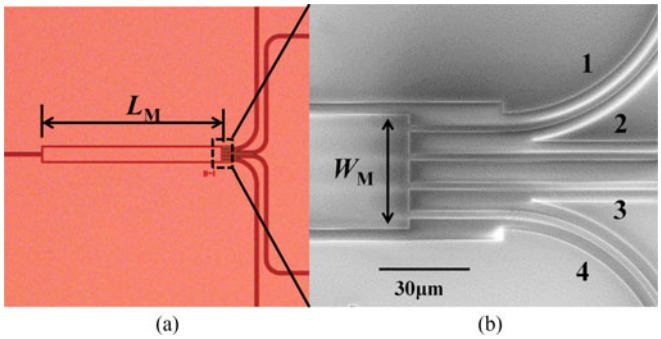

Fig. 2. (a) Schematic structure of the MMI coupler and (b) the SEM image of the output ports.

The multimode waveguide length of the 1 × 4 MMI coupler in TE polarization can be given as [20]

$$W_e = W_M + (\lambda_0/\pi)(n_{eff}^2 - n_c^2)^{-(1/2)} \quad (1)$$

$$L_M = n_{eff} W_e^2 / 4\lambda_0 \quad (2)$$

where $\lambda_0 = 1570$ nm is the central wavelength of the MMI coupler, $n_{\text{eff}} = 2.78$ and $W_{\text{M}} = 30\,\mu$m are the effective index and width of the multimode waveguide, respectively. Here, $n_{\text{r}} = 3.43$ and $n_{\text{c}} = 1.45$ refer to the refractive indices of Si and SiO_2, respectively. W_e is the effective width which takes into account the (polarization-dependent) lateral penetration depth of fundamental mode field, associated with the Goose-Hahnchen shifts [20]. It should be noted that although the lateral penetration depth in high-index contrast SOI structure is only 0.2 μm wide, the difference in L_{M} can be several micrometers, thus the Goose-Hanchen shift should not be ignored. According to the structure parameters above, the fabricated waveguide length is $L_{\text{M}} = 400\,\mu$m. The total length of the fabricated 1 × 4 optical switch is about 500-μm-long without the coupling waveguides and the metal electrodes, which is in the same level as the broadband cascaded 1 × 4 MZI based switches [8], [9]. Here, the large length is mainly caused by the MMI coupler. Since the length of the MMI coupler is inversely proportional to the output port number, the length of the MMI based switches can be greatly reduced for large-scale switch function, which will be much smaller than the cascaded MZI based devices. It should be noted that the width of the MMI coupler is not optimized in this work, and a better performance can be obtained after optimizations based on Ref. [21] in the future work. Since the MMI performance degrades when the ratio $W\text{port}/W_{\text{M}}$ decreases [21], the MMI coupler can be optimized by narrowing the waveguide width for a shorter length and widen the access ports for lower power imbalance, higher bandwidth and higher tolerance to fabrication errors. Wport is the width of the access port.

We demonstrate a W2 PCW based optical switch to achieve broadband switching function in each channel. Here, "W2" represents the line-defect width of the PCW, which equals to two rows of missing holes [15]. The SEM image of the fabricated W2 PCW is shown in Fig. 3(a), with a footprint of 17.6 μm × 8 μm. The lattice period (a) and hole radius (r) of the W2 PCW are set to $a = 440$ nm and $r = 146$ nm, respectively.

The switching function is performed by shifting the mini-stop band (MSB) [22] of the W2 PCW with thermo-optic effect. Fig. 3(b) shows the calculated dispersion curves of the W2 PCW in transverse electric (TE) polarization using plane wave expansion (PWE) method. The MSB effect is generated by the mode coupling between the basic mode and the second mode and performs as a broadband transmission dip in the transmission spectrum. It should be note that although the MSB is above the light line, the mode leakage will not remarkably affect the transmission loss due to the short PCW length [15]. Fig. 3(c) shows the finite-difference time-domain (FDTD) method calculated and experimentally measured transmission spectra of the W2 PCW, which are in good agreement. The transmission dip is as wide as 20 nm around a central wavelength of 1550 nm. Since Si has

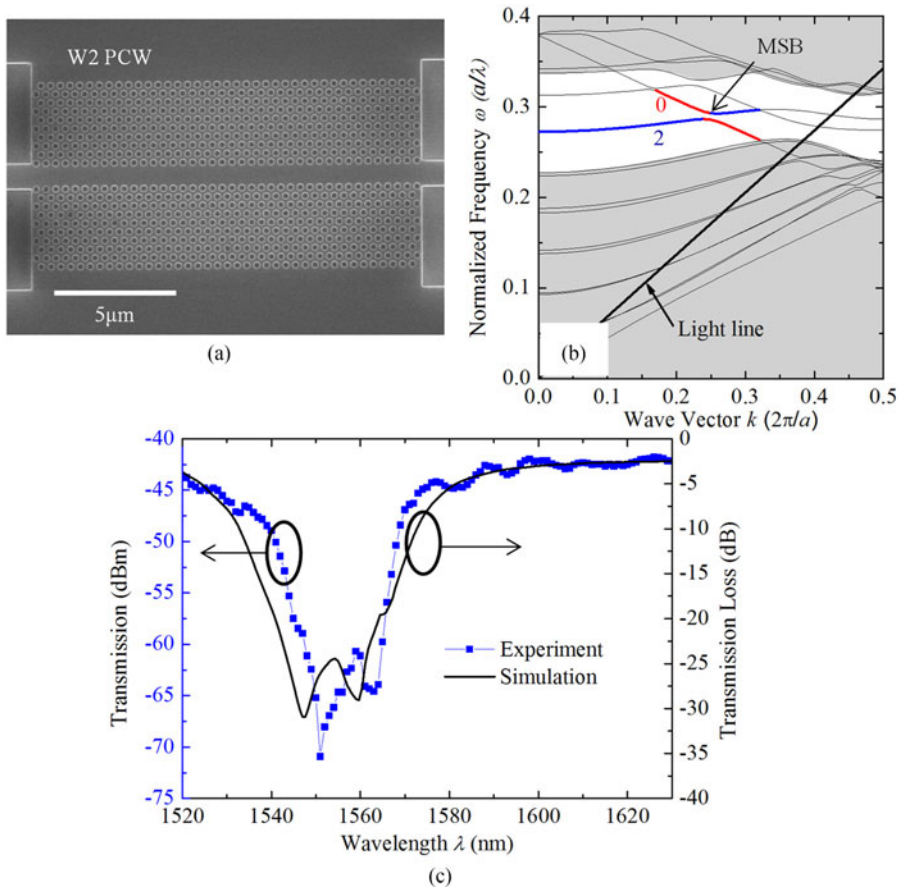

Fig. 3. (a) SEM image and (b) photonic band diagram of the W2 PCW. (c) Simulated and measured transmission spectra of the W2 PCW.

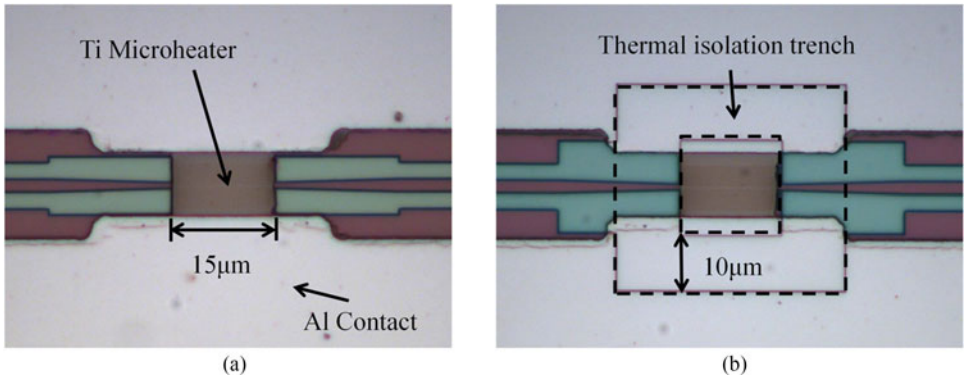

Fig. 4. Optical microscope image of the W2 PCW based switch (a) without and (b) with thermal insulation trench.

strong thermo-optic effect with a coefficient of $\Delta n/\Delta T = 1.86 \times 10^{-4}\,\mathrm{K}^{-1}$ [23], such an effect can provide tens of nanometer level wavelength shift to support the broadband switching function.

To enhance the tuning stability under large heating power, a slab Ti/Al microheater is applied, as shown in Fig. 4(a). The Ti heater has a footprint of 15 μm × 12 μm and is 100 nm thick. The 300 nm-thick Al contracts are located on both sides of the Ti heater. This slab microheater

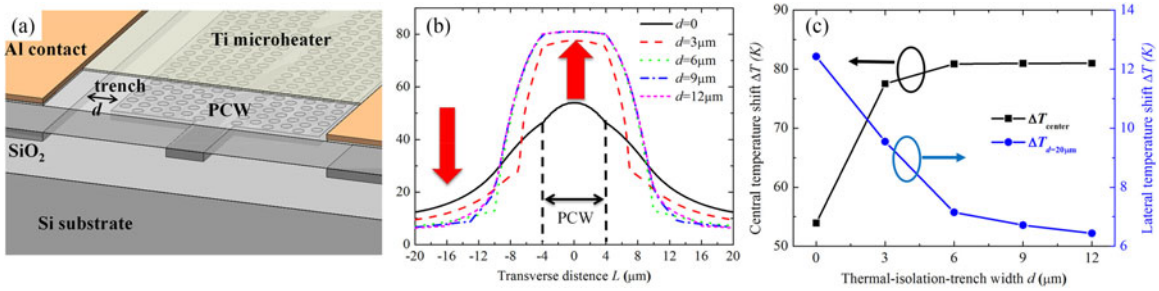

Fig. 5. (a) Schematic picture of the PCW switch. (b) Calculated temperature distributions of the PCW with different trench width. (c) Variation of the temperature shift in the center and lateral 20 μm away with different trench width.

provides a power limit larger than 150 mW and high heating transfer efficiency, which has been analyzed in our previous work [15], [24].

For dense multi-channel applications, inter-channel thermal crosstalk should be suppressed. However, since the silicon (Si) material has large thermo-optic effect, the optical switch is sensitive to the temperature shift [25]. The thermal conductivity of SiO_2 is two orders of magnitude smaller than that of Si. Therefore we introduce silicon dioxide (SiO_2) based compact and effective thermal insulation trenches surrounding each channel. Here, Si layer surrounding the PCW is etched and filling with SiO_2 to performs as thermal insulators, as shown in Fig. 4(b).

The trench is designed with consideration of the large difference in thermal conductivity between Si (138 W/m·K) and SiO_2 (1.4 W/m·K). The performance of the thermal insulation trench is analyzed using three-dimensional (3D) finite element method (FEM). We build the electro-thermos coupling model with different trench width and calculate the temperature distribution. The center of the PCW is heated up to a temperature change of $\Delta T = 53$ K, which refers to a typical refractive shift of $\Delta n = 0.01$. Fig. 5(a) presents the schematic picture of the PCW switch. Keeping the microheater structure and heating power unchanged, we change the trench width (d) around the PCW from 0 to 12 μm. Here, we just calculate the temperature distribution in centerline of the cross-section of the PCW to evaluate the effectiveness of the trench in heat confinement and efficiency enhancement, because the vertical temperature difference in Si PCW can be ignored with a thin film and a large thermal conductivity based on our previous work [22]. Fig. 5(b) shows the calculated temperature distributions of the PCW with different trench width, where L refers to the transverse distance to the PCW center. It can be observed that, after introducing the thermal insulation trenches, the temperature changes slightly in PCW slab ($L < 4$ μm) but drops sharply in the trench area ($L > 4$ μm), which evidences the effectiveness of the thermal insulation. Moreover, the temperature shift becomes larger in the PCW slab ($L < 4$ μm) and smaller out of the trench area ($L > 15$ μm) when trench is broadened, which evidences the validity of heating power confinement. Fig. 5(c) shows the temperature shift in the center and 20 μm away laterally, which are supposed to the temperature shift from the switch itself to a desired adjacent device. When broadening the trench width from 0 to 12 μm, the temperature shift increases by 50% in the center, from 53 K to 80 K, and decreases by 50% at adjacent device, from 13 K to 6.5 K.

3. Experimental Results

The switch performance is measured using an auto-aligned system, as shown in Fig. 6(a). The continuous light from a tunable laser is first set to TE polarization by a polarization controller, and then the light is coupled with the proposed structure by tapered lensed fibers. The output signal is measured by the power meter and oscilloscope. Fig. 6(b) shows the measured transmission spectra of the four channels and a reference single W2 PCW without heating power. Compared with the reference W2 PCW, the 1 × 4 MMI coupler introduces about 7.5 dB insertion

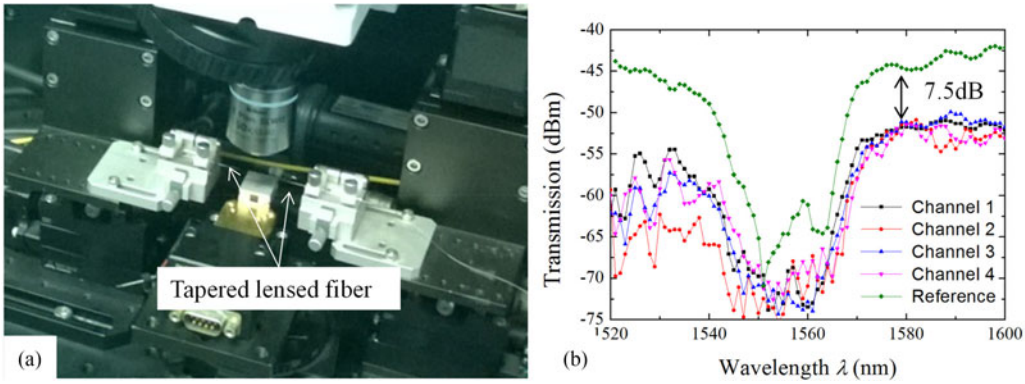

Fig. 6. (a) Auto-aligned coupling system. (b) Transmission spectra of the four channels and a referenced single W2 PCW.

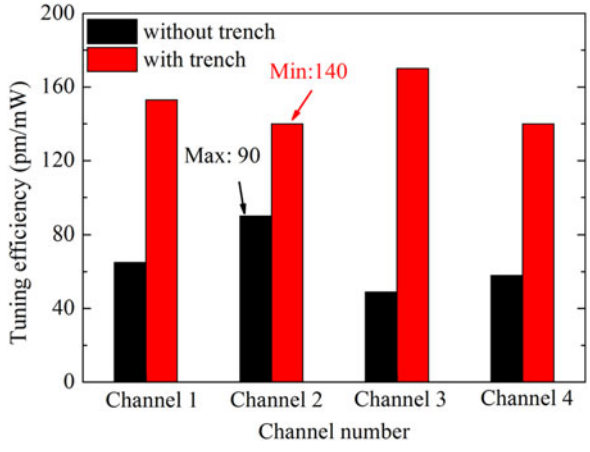

Fig. 7. Experimental results of the tuning efficiency with and without the thermal insulation trench.

loss to a single channel around 1570 nm, including 6 dB intrinsic loss and 1.5 dB scattering loss caused by fabrication roughness.

The tuning efficiency, defined as the ratio of the wavelength shift to the tuning power [3], are measured applying direct current voltage on each microheater. The experimental results of the tuning efficiency with and without the thermal insulation trench are shown in Fig. 7. Under the same tuning power (108 mW), the highest measured tuning efficiency of the switches without thermal insulation trenches is only 90 pm/ mW, while the lowest tuning efficiency of the switches with 10-μm-wide thermal insulation trenches is 160 pm/ mW. The experimental results show that the thermal insulation trench can increase the tuning efficiency by at least 77% (from 90 pm/ mW to 160 pm/ mW). It is a little higher than the simulation result (50%), which is because of the difference in thermal conductivity between the SOI wafer and that used in simulation.

Fig. 8(a)–(d) show the measured transmission spectra of each channel under different tuning power with an optimized trench width of 10 μm. Applying heating power up to 108 mW on each switch, the redshift of the four channels are up to 20.5 nm, 19.4 nm, 17.3 nm, and 18.4 nm. This indicates that the broadband switching function has been achieved in all channels. In fact, the designed slab microheater can afford tuning power up to 150 mW, which provides more than 24 nm tuning range [15]. Here, we stopped at 108 mW for a 15 nm bandwidth and the stability of the device. When the selected PCW switch is in " On" state, the light goes through the PCW. When it is in the "Off" state, the input light meets the MSB dip and is reflected and scattered at the interface

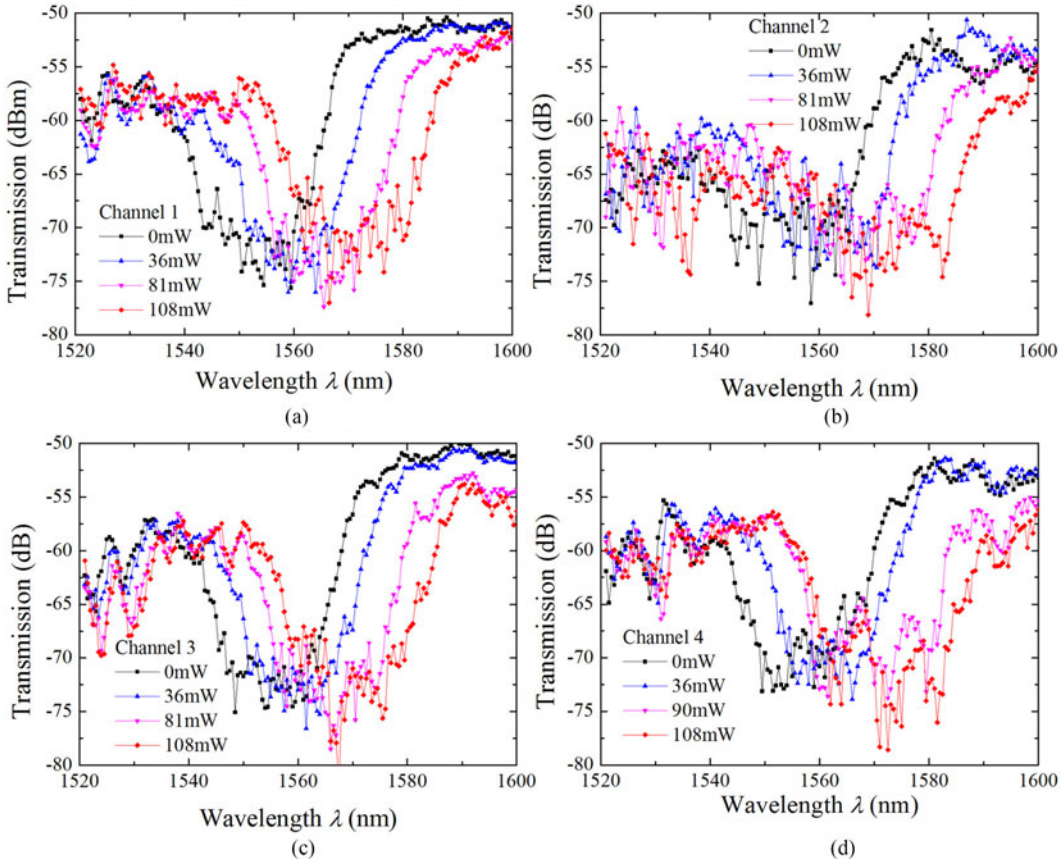

Fig. 8. (a)–(d) Transmission spectra shift of the four channels under a tuning power up to 108 mW.

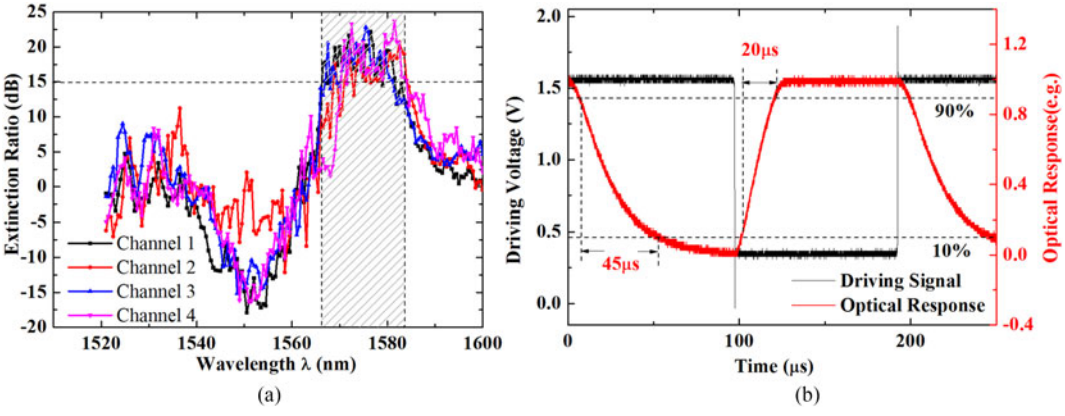

Fig. 9. (a) Extinction ratio of the four channels under a tuning power of 108 mW and (b) dynamic optical response of the switch.

of the PCW. Here, no reflection to the MMI is observed in the measurements, and therefore, the light reflected back to the waveguide is only a small part and will not affect the performance of the device.

Fig. 9(a) shows the extinction ratio of each switch channel under a tuning power of 108 mW. Each channel is at on-state without power and turned to off-state with 108 mW applied. If we set the switch threshold value as an extinction ratio of 15 dB, the operating wavelength can be found

from 1565 nm to 1584 nm. It can be concluded from the measured results that all the four channels have operating bandwidths of 15 nm ± 1 nm while the extinction ratio is higher than 15 dB, and the overlapping wavelength region is from 1570.3 nm to 1581.3 nm. According to the measured optical response shown in Fig. 9(b), the rising and falling time is 20 μs and 45 μs, respectively, which corresponds to a switch speed of 15 kHz. According to [15], the power consumption can be estimated by assuming the channel spacing and data rate as 0.4 nm (50 GHz Grid) and 10 Gb/s, according to the International Telecommunication Union (ITU) standard. For our demonstrated device, the heating power is 108 mW within the wavelength span of 15 nm, and therefore, the power consumption per bit is only 0.29 pJ/bit.

4. Conclusions

In conclusion, we have demonstrated a 1 × 4 broadband thermo-optic switch. The operation bandwidth of the four channels could be as broad as 15 ± 1 nm (within the wavelength range of 1565–1580 nm) with the extinction ratio of more than 15 dB. A compact W2 PCW based switch is located in each channel with a PCW footprint of only 17.6 μm × 8 μm. Thermal-isolation-trenches are also introduced, which increase the thermo-optic tuning efficiency by at least 77% in experiment. Due to the 6 dB intrinsic loss introduced by the MMI coupler, the insertion loss of the proposed switch is larger than the cascaded microring resonator based switches and the Mach-Zender interferometer (MZI) based switches. However, compare to the latter two types of switches, the MMI switches provide a better trade-off between the bandwidth and the footprint. The experimental results indicate the potential of the demonstrated 1 × 4 broadband thermo-optic switch in silicon on-chip interconnects.

References

[1] D. Miller, "Device requirements for optical interconnects to silicon chips," *Proc. IEEE*, vol. 97, no. 7, pp. 1166–1185, Jul. 2009.

[2] X. Luo, J. Song, and S. Feng, "Silicon high-order coupled-microring-based electro-optical switches for on-chip optical interconnects," *IEEE Photon. Technol. Lett.*, vol. 24, no. 10, pp. 821–823, May 2012.

[3] X. Zheng *et al.*, "A tunable 1 × 4 silicon CMOS photonic wavelength multiplexer/demultiplexer for dense optical interconnects," *Opt. Express*, vol. 18, pp. 5151–5160, 2010.

[4] J. Van Campenhout and W. Green, "Low-power, 2Î2 silicon electro-optic switch with 110-nm bandwidth for broadband reconfigurable optical networks," *Opt. Exp.*, vol. 17, no. 26, pp. 767–769, 2009.

[5] W. Wang, H. Zhou, J. Yang, M. Wang, and X. Jiang, "Highly integrated 3 × 3 silicon thermo-optical switch using a single combined phase shifter for optical interconnects," *Opt. Lett.*, vol. 37, no. 12, pp. 2307–2309, Jun. 2012.

[6] L. Chen and Y. Chen, "Compact, low-loss and low-power 8 × 8 broadband silicon optical switch," *Opt. Exp.*, vol. 20, no. 17, pp. 18977–18985, 2012.

[7] Y. Vlasov, W. M. J. Green, and F. Xia, "High-throughput silicon nanophotonic wavelength-insensitive switch for on-chip optical networks," *Nat. Photon.*, vol. 2, no. 4, pp. 242–246, Mar. 2008.

[8] G. Calo, A. D'Orazio, and V. Petruzzelli, "Broadband mach-zehnder switch for photonic networks on chip," *J. Lightw. Technol.*, vol. 30, no. 7, pp. 944–952, Apr. 2012.

[9] S. Chen, Y. Shi, S. He, and D. Dai, "Low-loss and broadband 2 × 2 silicon thermo-optic Mach-Zehnder switch with bent directional couplers," *Opt. Lett.*, vol. 41, no. 4, pp. 836–839, 2016.

[10] F. Cuesta-Soto *et al.*, "All-optical switching structure based on a photonic crystal directional coupler," *Opt. Exp.*, vol. 12, no. 1, pp. 161–167, 2004.

[11] N. Yamamoto, T. Ogawa, and K. Komori, "Photonic crystal directional coupler switch with small switching length and wide bandwidth," *Opt. Exp.*, vol. 14, no. 3, pp. 1223–1229, 2006.

[12] D. M. Beggs, T. P. White, L. O'Faolain, and T. F. Krauss, "Ultracompact and low-power optical switch based on silicon photonic crystals," *Opt. Lett.*, vol. 33, no. 2, pp. 147–149, Jan. 2008.

[13] Y. A. Vlasov, M. O'Boyle, H. F. Hamann, and S. J. McNab, "Active control of slow light on a chip with photonic crystal waveguides," *Nature*, vol. 438, no. 7064, pp. 65–69, Nov. 2005.

[14] L. O'Faolain, D. M. Beggs, T. P. White, T. Kampfrath, K. Kuipers, and T. F. Krauss, "Compact optical switches and modulators based on dispersion engineered photonic crystals," *IEEE Photon. J.*, vol. 2, no. 3, pp. 404–414, Jun. 2010.

[15] K. Cui, X. Feng, Y. Huang, Q. Zhao, Z. Huang, and W. Zhang, "Broadband switching functionality based on defect mode coupling in W2 photonic crystal waveguide," *Appl. Phys. Lett.*, vol. 101, no. 15, 2012, Art. no. 151110.

[16] A. Hosseini, D. Kwong, and C. Lin, "Output formulation for symmetrically excited one-to-multimode interference coupler," *IEEE J. Sel. Top. Quantum Electron.*, vol. 16, no. 1, pp. 61–69, Jan./Feb. 2010.

[17] K. Cui *et al.*, "Thermo-optic switch based on transmission-dip shifting in a double-slot photonic crystal waveguide," *Appl. Phys. Lett.*, vol. 100, no. 20, 2012, Art. no. 201102.

[18] Q. Zhao, K. Cui, X. Feng, F. Liu, W. Zhang, and Y. Huang, "Variable optical attenuator based on photonic crystal waveguide with low-group-index tapers," *Appl. Opt.*, vol. 52, no. 25, pp. 6245–6249, 2013.
[19] A. Hosseini, H. Subbaraman, D. Kwong, Y. Zhang, and R. T. Chen, "Optimum access waveguide width for 1 × N multimode interference couplers on silicon nanomembrane," *Opt. Lett.*, vol. 35, no. 17, pp. 2864–2846, Sep. 2010.
[20] L. B. Soldano and E. C. M. Pennings, "Optical multi-mode interference devices based on self-imaging: Principles and applications," *J. Lightw. Technol.*, vol. 13, no. 4, pp. 615–627, Apr. 1995.
[21] P. A. Besse, M. Bachmann, H. Melchior, L. B. Soldano, and M. K. Smit, "Optical bandwidth and fabrication tolerances of multimode interference couplers," *J. Lightw. Technol.*, vol. 12, no. 6, pp. 1004–1009, Jun. 1994.
[22] K. Cui *et al.*, "Temperature dependence of ministop band in double-slots photonic crystal waveguides," *Appl. Phys. Lett.*, vol. 95, no. 19, 2009, Art. no. 191901.
[23] G. Cocorullo and I. Rendina, "Thermo-optical modulation at 1.5 μm in silicon etalon," *Electron. Lett.*, vol. 28, no. 1, pp. 83–85, 1992.
[24] Q. Zhao, K. Cui, Z. Huang, and X. Feng, "Compact thermo-optic switch based on tapered W1 photonic crystal waveguide," *IEEE Photon. J.*, vol. 5, no. 2, 2013, Art. no. 2200606.
[25] C. Batten *et al.*, "Building many-core processor-to-DRAM networks with monolithic CMOS silicon photonics," *IEEE Micro*, vol. 29, no. 4, pp. 8–21, Jul./Aug. 2009.